

See discussions, stats, and author profiles for this publication at: <https://www.researchgate.net/publication/51762008>

# Physicochemical Characterization of Solute Retention in Solvent Resistant Nanofiltration: the Effect of Solute Size, Polarity, Dipole Moment, and Solubility Parameter

ARTICLE *in* THE JOURNAL OF PHYSICAL CHEMISTRY B · NOVEMBER 2011

Impact Factor: 3.3 · DOI: 10.1021/jp207569m · Source: PubMed

---

CITATIONS

14

READS

29

---

## 8 AUTHORS, INCLUDING:



Elena Tocci

Italian National Research Council

40 PUBLICATIONS 477 CITATIONS

[SEE PROFILE](#)



Johannes Carolus (John) Jansen

Italian National Research Council

105 PUBLICATIONS 1,826 CITATIONS

[SEE PROFILE](#)



F. Tasselli

Italian National Research Council

46 PUBLICATIONS 588 CITATIONS

[SEE PROFILE](#)



Jan Degrève

University of Leuven

72 PUBLICATIONS 1,861 CITATIONS

[SEE PROFILE](#)

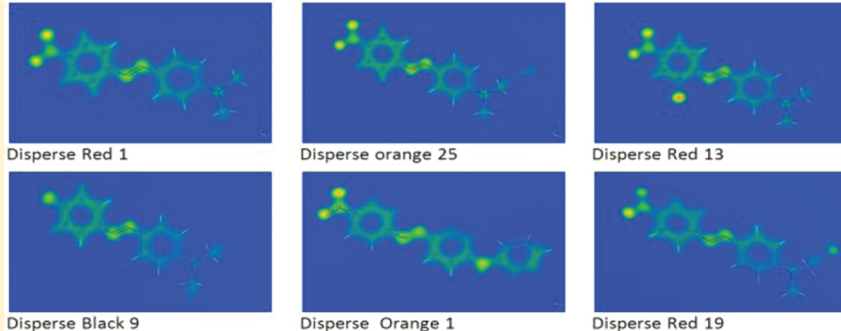
# Physicochemical Characterization of Solute Retention in Solvent Resistant Nanofiltration: the Effect of Solute Size, Polarity, Dipole Moment, and Solubility Parameter

Siavash Darvishmanesh,<sup>†</sup> Johan Vanneste,<sup>†</sup> Elena Tocci,<sup>‡</sup> Johannes Carolus Jansen,<sup>‡</sup> Franco Tasselli,<sup>‡</sup> Jan Degrève,<sup>†</sup> Enrico Drioli,<sup>‡</sup> and Bart Van der Bruggen<sup>\*,†</sup>

<sup>†</sup>Department of Chemical Engineering, Laboratory for Applied Physical Chemistry and Environmental Technology, Katholieke Universiteit Leuven, W. de Crooylaan 46, B-3001 Leuven, Belgium

<sup>‡</sup>Institute on Membrane Technology (ITM-CNR), Via P. Bucci, 87030 Arcavacata di Rende, Cosenza, Italy

## ABSTRACT:



Growing interest in nanofiltration for solvent purification requires a fundamental understanding of the physicochemical mechanisms of solute retention in organic solvent nanofiltration. In this study, the retention of a similar series of azo dyes with approximately similar molar mass (around 350 Da) by four nanofiltration membranes was studied. The membranes used are commercially available polymeric nanofiltration membranes with molecular weight cutoff between 150 and 300 Da (DuraMem150, StarMem122, NF270 and Desal-Dk). In order to correlate the retention with the size of the molecules, use was made of different parameters for the molecular size: molar mass, the Stokes diameter, the equivalent molar diameter, and the cavity surface in methanol and ethanol. All parameters were calculated by using molecular dynamics simulations. For each size parameter, the correlation with retention in nanofiltration experiments was calculated. For the StarMem122 membrane, zero retentions were observed due to the swelling of the membrane and pore size enlargement in methanol and ethanol. For the three other membranes, a fairly good correlation of the retention with the size could only be observed if the size difference between compounds is sufficiently large. Two other factors were studied by using molecular dynamics, i.e., the polarity of the molecule and the electron density of the molecule. The importance of these factors depends on the structure of the molecule as well as the functional groups of the polymer. A very good correlation has been observed for retention of dyes versus their dipole moment. Finally, the effect of solubility parameters of dyes on their retention did not show any significant effect.

## 1. INTRODUCTION

Over the past decade, solvent resistant nanofiltration (SRNF) emerged as a new and promising membrane process. SRNF allows saving energy compared to traditional separation units in organic solvent purification.<sup>1</sup> SRNF, also known as organophilic nanofiltration, is comparable to conventional nanofiltration, but the membranes used are stable in organic solvents. While membrane manufacturers have developed high-performance SRNF membranes (Evonik, Solsip and Koch), transport and separation data for SRNF membranes are not well reported in the literature, and the mechanism of transport through SRNF membranes is not well understood. Numerous

studies have been undertaken to apply nanofiltration (NF) membranes for the removal of solutes from aqueous media.<sup>2</sup> Transport mechanisms and process drawbacks are relatively well understood for aqueous nanofiltration systems.<sup>3</sup> It was found that separation of organic molecules, pharmaceuticals, dyes, metal ions, and contaminants from water mainly occurs through size exclusion in addition to charge interactions.<sup>4</sup> NF membranes, which bridge ultrafiltration (UF) and reverse

**Received:** August 7, 2011

**Revised:** October 31, 2011

**Published:** November 01, 2011



**Table 1. Organic Solvent with the Most Important Physical Properties.<sup>38</sup>**

solvent	molar mass (g/mol)	viscosity @ 25 °C mPa·s	surface tension @ 20 °C mN/m	dielectric constant @ 20 °C
methanol	32.00	0.54	22.12	33.00
ethanol	46.10	1.08	21.99	24.90

**Table 2. Membranes Used in This Study and Membrane Characteristics**

membrane	manufacturer	pore size, MWCO	membrane class	material
Desal-DK	GE Osmonics	150–300 Da	NF (dense)	PA
NF270	Dow/FilmTec	200–300 Da	NF (dense)	PA
DuraMem150	Evonik	150 Da	SRNF (Dense)	X-PI

osmosis (RO) membranes, are specified to be porous, with a typical pore diameter of 1–3 nm. Generally NF membranes have nominal “molecular weight cutoff” (MWCO), which is the molar mass of a solute retained for 90%, between 100 and 1000. In addition to this, SRNF has been introduced during the past decade for potential application in organic media. Unfortunately, the removal of organic solutes from organic solvents using membrane technology has been addressed by very few researchers,<sup>5–10</sup> and little is known of the fundamental transport and separation mechanisms.<sup>11–15</sup> For aqueous nanofiltration, retention and permeation performance of a given membrane can be estimated according to the molecular size of solutes.

Machado et al.<sup>16</sup> examined solvent fluxes (for alcohols, paraffins, acetone, and water) and presented a model describing solvent transport through SRNF membranes (MPF-50, MWCO 700, Koch, USA). They did not observe a clear correlation between the flux and the solvent molar volume, although a flux decrease was found within a homologous series of linear alcohols with increasing molecular volume. It was, however, not clear whether this decrease should be attributed to the By contrast, Bhanushali et al.<sup>17</sup> suggested a linear relationship with the molar volume, as an indirect measure for the solvent diffusivity in the membrane matrix. Reddy et al.<sup>18</sup> reported a minor effect of the molecular structure on the solvent permeability: branched alcohols showed lower fluxes than analogous linear alcohols. Finally, Machado et al.<sup>19</sup> found important indications that, apart from viscous forces, surface properties can have an effect on the solvent permeability as well. In analogy to transport of solvent molecules from one medium to another, a surface resistance is assumed to be proportional to the difference in surface tension between the liquid solvent and the membrane top layer. Later on, Bhanushali et al.<sup>17</sup> also used the membrane surface tension to describe repulsion and attraction forces at the membrane–solvent interface, in combination with a sorption value of the solvent on the membrane material. Vankelecom et al.<sup>20</sup> suggested that membrane swelling might be used as a measure for the membrane–solvent interactions. Robinson et al.<sup>21</sup> suggested the use of the Hildebrand solubility parameters of the solvent and the membrane to describe these interfacial interactions. They proposed that both viscosity and surface tension are key parameters in solvent permeability through the membrane. Whu et al.<sup>22,23</sup> investigated SRNF in methanol solutions using the SRNF membrane from Koch (MPF series) and reported lower retentions than can be assumed based on the MWCO values claimed

by the manufacturer. Recently, Darvishmanesh et al.<sup>24–26</sup> incorporated three parameters, namely, viscosity, surface tension, and dielectric constant, into the transport equation. Later on they also found that the solubility parameter also plays an important role in transport of solvents through selected SRNF membranes.<sup>1,11</sup> However, to develop a general mathematical model for solute transport in SRNF, a general understanding of transport of solutes and solvents through SRNF membranes is necessary. Systematic studies to identify solute transport mechanisms have been initiated already. Yang et al.<sup>27</sup> reported the flux, retention, and stability of NF membranes with aqueous and organic solvents (methanol, ethyl acetate, toluene), and three selected solutes having the same molar mass (Orange II, Safranine O, and Solvent Blue 35). They showed that the nominal MWCO is only valid for predicting the retention in aqueous solutions, and that the retention in organic solvents either for molecules of the same molar mass or even for the same molecule is unpredictable and depends on the specific solvent. It was found that solute retention in organic solvents is lower than in aqueous solution, and that the solvent has a significant influence on the retention. Darvishmanesh et al.<sup>1</sup> studied the effect of solvent on solute molecular size. It was shown that the effective size of a molecule is dependent on the solvent due to solvation and hydration of the solute by the solvent. The size of the solute in the solvent from a similar chemical family was studied separately. They showed that the retention was influenced by the molecular size of the solute in the same group of solvents. It was found that in a system comprising the solvent, solute and membrane, interactions between solvent and membrane have much more effect on separation than solvent–solute interactions. The effect of chemical functional groups present in the solute on retention in SRNF is an interesting area where information is still lacking.

Nowadays advanced improvements in the computational field are used to understand the mechanistic view of complex molecules and polymeric systems via superior methods such as molecular mechanics and dynamics.<sup>31–33</sup> Molecular dynamics (MD) has a good record of making predictions of the values of the fractional free volume (FFV), fractional accessible volume (FAV), and cavity size distribution of membranes that are in good agreement with experimental data.<sup>34–37</sup> Choi et al.<sup>28</sup> and Kavassalis et al.<sup>29</sup> demonstrated the use of molecular modeling in estimating the solubility parameters of nonionic surfactants. In a recent study published by Simperler et al.,<sup>30</sup> MD simulations were used to determine the glass transition temperatures of carbohydrates.

The current study is targeted at understanding transport characteristics of solutes with similar molecular weight and shape (structure) but different chemical functional groups through commercially available SRNF membranes.

## 2. MATERIALS AND METHODS

**Solvent.** Two organic solvents, methanol and ethanol, were selected for this study since all selected membranes (below) are stable in these solvents while all solutes are soluble in them. Table 1 lists the physical-chemical properties of the solvents used.<sup>38</sup>

**Membranes.** NF and SRNF membranes selected for this study are listed in Table 1, which shows the most important properties. NF270 and Desal-DK are membranes designed for application in aqueous systems but are also claimed to be stable in methanol and ethanol. Both membranes are thin film composite

Table 3. Principle Characteristics of the Dyes Used in This Study

	molar mass	charge	dye content	UV absorption $\lambda_{\text{max}}$ nm in methanol	UV absorption $\lambda_{\text{max}}$ nm in ethanol	density
Disperse Red 1	314.34	neutral	95%	496.4	481.4	1.230
Disperse Orange 25	323.35	neutral	95%	473.4	457.4	1.191
Disperse Red 13	348.78	neutral	95%	513.6	504.4	1.308
Disperse Black 9	300.36	neutral	97%	448.6	442.2	1.229
Disperse Orange 1	318.33	neutral	15%	470.6	473.8	1.241
Disperse Red 19	330.34	neutral	95%	484.4	479.8	1.301
Disperse Red 1 methacrylate	382.41	neutral	95%	491.2	487.3	NA <sup>a</sup>
Disperse Red 13 methacrylate	416.86	neutral	98%	203.1	201.2	NA

<sup>a</sup> NA: Not available.

membranes with polyamide (PA) as the top-layer.<sup>39</sup> DuraMem150 membranes are solvent stable membranes, specifically designed for application in organic solvents. StarMem122 membranes are polyimide (PI) membranes prepared by immersion precipitation. DuraMem membranes are PI membranes modified via treatment with diamines for cross-linking to improve their stability in apolar solvent (X-PI). All membranes were supplied in a dry form.

**Solutes.** Eight different azo-dyes (Aldrich, UK), all with a molecular size in range of 300–350 Da, around the nominal MWCO range (150–400) of the selected NF and SRNF membranes (Table 2), were used. These dyes are very similar in structure. Two methacrylate azo dyes with larger size and a similar structure were used to investigate the size effect more precisely. The physicochemical characteristics of these dyes are given in Table 3, and the structures of the dyes are shown in Figure 1. Dyes were chosen as they are easy to detect using spectrophotometry.<sup>40</sup>

**Filtration Study.** Retention and permeability measurements were carried out using a Sterlitech HP4750 stirred cell (Sterlitech, USA). The cell consists of a cylindrical stainless steel vessel with removable end plates. A membrane disk was placed at the end of the cell supported by a porous stainless steel disk. The active membrane area was 16.9 cm<sup>2</sup>. The volume of the solution fed to cell above the membrane disk was 200 mL. The solution in the vessel was stirred by help of a Teflon-coated magnetic bar, located 3 mm above the membrane. The membrane was cut in a circular disk of 49 mm in diameter, and pretreated in the solvent of filtration solution overnight prior to filtration experiments. All experiments were carried out at ambient temperature and at a pressure of 20 bar. The cell was pressurized with compressed nitrogen gas. The volume of permeate was measured with a measuring cylinder. For experiments used to determine dye retention, the solution was stirred with a Teflon-coated magnetic stir-bar at 1000 rpm. Fluxes were determined by measuring the time difference,  $\Delta t$ , required to collect a certain volume of permeate,  $V_p$ . The flux can then be calculated from

$$J \left( \frac{l}{h \cdot m^2} \right) = \frac{V_p (ml) \cdot 3600 \left( \frac{s}{h} \right)}{1000 \left( \frac{ml}{l} \right) A (m^2) \cdot \Delta t (s)} \quad (1)$$

where  $A$  (m<sup>2</sup>) is the effective membrane area. Flux and retention was measured three times with a new membrane sheet

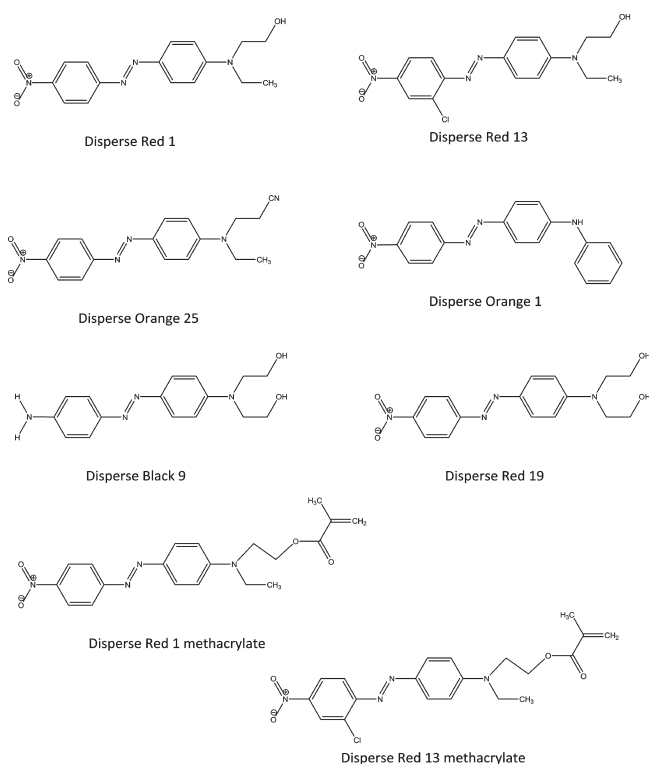


Figure 1. Molecular structures of selected dyes in this study.

for every experimental series. Prior to each experiment, pure solvent was filtered for at least 2 h to remove any trace of preserving material in the membrane, and to stabilize the flux.

Considerable differences in measured solvent flux were observed with different membrane samples in literature. These differences arise from the nonhomogeneity of the membrane sheets, i.e., variability in thickness, porosity, and pore size distribution of membrane sample area. In this study, in order to avoid effects of polymer “memory” on solvent permeation and neutralize the effect of filtration on the retention result and nonuniformity on the permeate flux, one membrane sample was used for all dyes. First, permeation of pure solvent at 20 bar was measured. Then the solution containing dyes was applied to the cell. Each retention test was continued until 50% of the feed solution permeated through the membrane. The flux of the test solution was then determined. To compare flux decline during

filtration, relative fluxes ( $R_F$ ) were defined as the ratio of permeate flux ( $J_v$ ) to pure solvent flux ( $J_S$ ).

$$R_F = \frac{J_v}{J_S} \quad (2)$$

Subsequently, pure solvent fluxes were measured to normalize the results. The normalized flux,  $J_n$  (dimensionless), was then

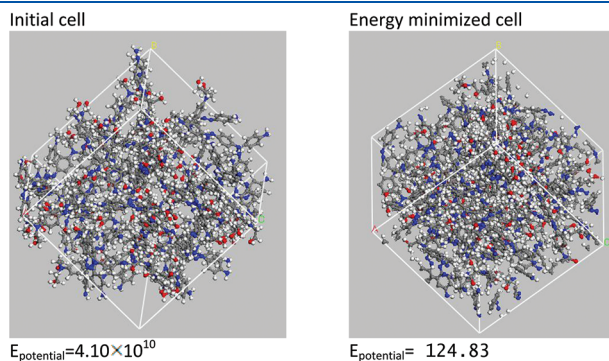


**Figure 2.** Comparison of an energy-minimized amorphous cell of Disperse Black 9 to its initial structure at 298 K after 1000 steps of minimization.

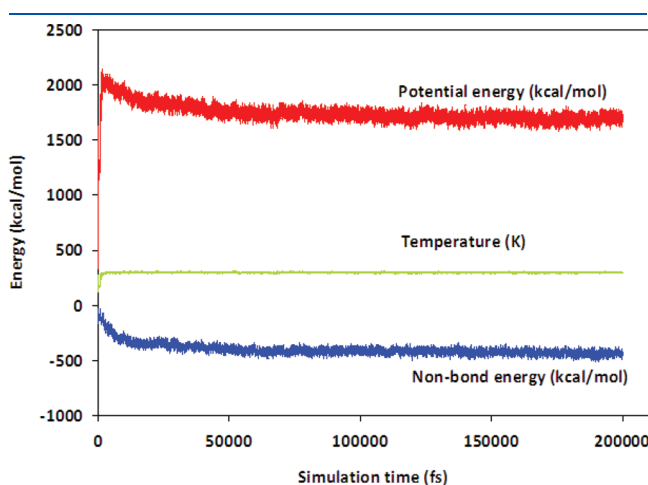


**Figure 3.** Total potential energy, non-bond energy, and temperature profile of Disperse Black as a function of MD simulation time.

expressed as the ratio of pure solvent flux after each filtration experiment to the initial pure solvent flux.

$$J_n = \frac{J_S}{J_S - \text{initial}} \quad (3)$$

The retention was calculated by

$$\text{Rej} = \left( 1 - \frac{C_p}{C_r} \right) \times 100 (\%) \quad (4)$$

where  $C_p$  and  $C_r$  are the final concentrations in the permeate and retentate, respectively. The maximum standard deviation in the concentration analysis was found to be <5%.

**MD Simulation and Calculation of the Molecular Descriptor by Molecular Modeling.** The MD simulations were performed using the molecular modeling package of Accelrys, Materials Studio 5.0.<sup>33</sup> In MD simulations, the microstates of a structure (in the phase space) are determined by the positions and momenta. The way in which the systems move through phase space is governed by Hamiltonian's equations or classically solving the Newtonian equation of motion (second law). The equations of motion are transformed to a time independent Hamiltonian function, which represents the total energy expressed as the sum of the kinetic and potential energies of the system. MD is a deterministic method by which the state of the system at any future time can be predicted from its initial (current) state.<sup>34</sup>

The molecular structures of azo dyes were obtained from the Cambridge Structural Database (Figure 1). The ab initio PCFF force field<sup>35</sup> was utilized for MD simulations. Ten *in silico* amorphous models ("amorphous cells") each for every azo dye were generated at 298 K, with periodic boundary conditions. The dimensions of the amorphous cells were 3 nm × 3 nm × 3 nm. The lowest energy configuration of the 10 amorphous cells for each compound was selected for energy minimization using the steepest decent and Fletcher-Reeves conjugate gradient procedures to remove unfavorable interactions and reach the lowest energy state.<sup>33</sup> Figure 2 shows the energy-minimized structure of the unit cell of Disperse Black 9 compared to its first configuration.

Later on the energy-minimized amorphous cells were used as an initial cell for the MD simulations (i.e., the equilibration stage). Following minimization, the amorphous cells were allowed to relax for 2 ns under isothermal (NVT) conditions at 298 K. An equilibration run of 2 ns is sufficient due to the constancy

**Table 4. Experimental Relative Flux, Normalized Flux, and Retention (Applied Pressure 20 bar)**

membrane	DuraMem150						NF270						Desal-Dk					
	methanol = 10.66			ethanol = 2.6			methanol = 100.39			ethanol = 36.20			methanol = 66.57			ethanol = 22.05		
Solvent initial flux	$R_F$	$J_n$	$R$ (%)	$R_F$	$J_n$	$R$ (%)	$R_F$	$J_n$	$R$ (%)	$R_F$	$J_n$	$R$ (%)	$R_F$	$J_n$	$R$ (%)	$R_F$	$J_n$	$R$ (%)
Disperse Red 1	1.03	0.95	97	1.02	0.98	97	0.96	1.03	78	1.02	1.01	74	0.99	0.99	89	0.98	0.95	85
Disperse Orange 25	0.99	0.98	97	1.00	0.99	96	0.99	0.95	79	0.99	1.03	73	0.97	1.01	95	0.97	0.98	91
Disperse Red 13	1.00	1.02	98	1.01	0.97	98	0.98	0.97	74	0.98	0.97	69	0.98	1.02	93	0.99	0.96	89
Disperse Black 9	0.98	0.97	91	1.02	1.01	92	1.01	0.98	22	1.02	0.95	30	1.02	0.99	59	1.02	0.95	61
Disperse Orange 1	0.97	0.99	96	0.98	0.97	97	1.02	0.98	72	0.97	1.00	74	0.96	1.04	93	1.00	0.98	97
Disperse Red 19	0.99	0.96	95	0.97	0.98	96	0.99	0.99	63	1.01	1.01	64	0.97	0.99	87	0.96	0.99	88
Disperse Red 1 me	1.01	0.92	99	0.96	0.97	99	1.03	1.01	84	0.96	0.98	81	0.95	0.95	98	1.01	1.00	98
Disperse Red 13 me	0.98	0.97	99	0.99	0.99	99	0.96	1.03	89	0.99	0.99	86	0.98	0.98	99	0.97	0.99	98

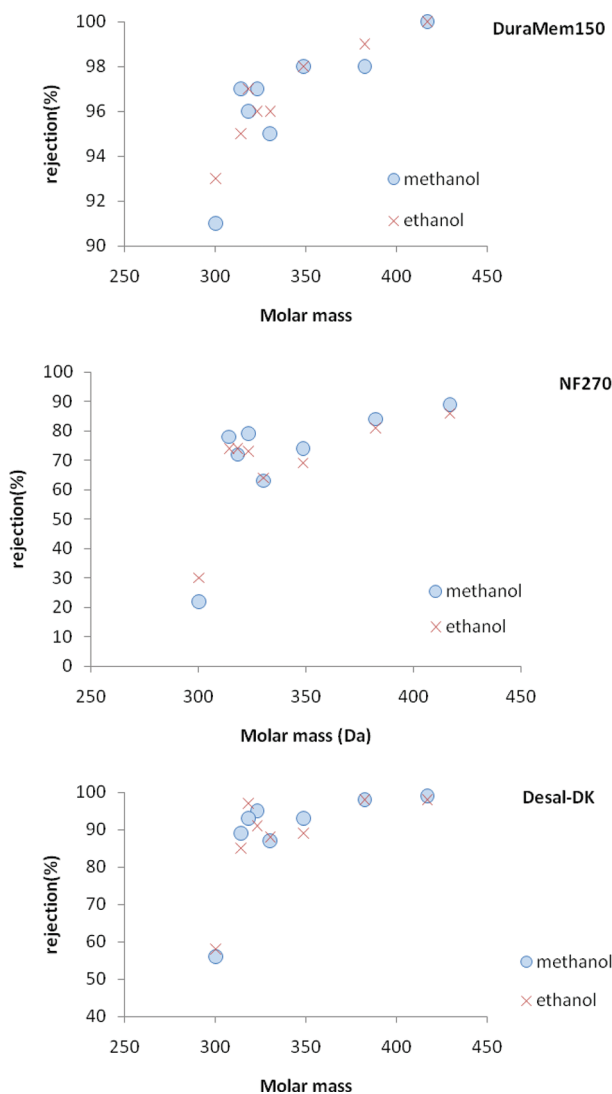


**Figure 4.** Retention curves as a function of molecular weight for the membranes DuraMem150, NF270, and Desal-DK. (applied pressure: 20 bar). Retentions of dyes are presented for both methanol and ethanol. From left to right: Disperse Black 9, Disperse Red 1, Disperse Orange 1, Disperse Orange 25, Disperse Red 19, Disperse Red 13, Disperse Red 1 methacrylate, Disperse Red 13 methacrylate.

in the density value obtained. Later on, the equilibrated structure was processed under NVT conditions followed by application of the NPT dynamic to allow cells to reach their equilibrium density for 100 ps at 298 K with a time step of 1 fs. The equilibration time is related to the number of atoms in each individual structure. MD was continued until the total energy of each structure had become stable. The time evolution energy profiles during MD simulations of Disperse Black 9 are presented in Figure 3. Figure 3 shows that a duration of 2 ns was adequate to reach the equilibration without any significant deviation in the density of each structure. The nonbonded van der Waals and electrostatic interactions were truncated using a group-based cutoff (van der Waals cutoff = 14). Trajectory frames were captured during the production run, and the data from the final 100 ps were used for computing the cohesive energy density and solubility parameter for the compound.

**Table 5. Calculated Dimensions in Terms of van der Waals Surface and Occupied Volume**

	in methanol		in ethanol	
	surface area <sup>a</sup> (Å <sup>2</sup> )	occupied volume (Å <sup>3</sup> )	surface area <sup>a</sup> (Å <sup>2</sup> )	occupied volume (Å <sup>3</sup> )
Disperse Red 1	284.65	285.1	287.83	285.29
Disperse Orange 25	316.09	297.07	327.59	300.48
Disperse Red 13	292.36	296.36	307.19	291.13
Disperse Black 9	300.08	278.05	248.31	274.18
Disperse Orange 1	243.75	279.35	300.55	274.64
Disperse Red 19	318.63	292.57	298.41	295.99
Disperse Red 1 me	386.4	346.76	339.76	346.61
Disperse Red 13 me	388.93	357.25	351.68	355.36

The density of a final cell after simulation is compared to experimental density. The simulated values are in complete agreement with the experimental data. The close agreement between the two density values signifies the effective optimization of intermolecular interactions achieved between the molecules and, thus, its packing in reality within the structures.

The electron density field and dipole moment of azo dyes in methanol and ethanol was optimized with a semiempirical molecular orbital package for a molecular organic and inorganic systems module in Materials Studio called VAMP. This module implements the density functional theory as well. VAMP uses two different models for solvation: numerical self-consistent reaction field (SCRF) calculations,<sup>41</sup> and a conductor-like screening model (COSMO).<sup>42</sup> Such models are essential for understanding the properties of molecules in solution and are easily included in VAMP calculations. VAMP determines a molecular wave function, which can then be used to derive molecular properties such as energy and dipole moments.

The dipole moment  $\mu$  of a molecule is the addition of the permanent dipole moment  $\mu^{\text{per}}$  to the induced dipole moment  $\mu^{\text{ind}}$ . The permanent dipole moment is about constant, while the induced dipole moment is relative to the electrical field. Since the electrical field induced by the charge of the membranes could be assumed small (organic solvent medium), the induced dipole moment can be neglected. The permanent dipole moment  $\mu^{\text{per}}$  of the uncharged molecules was calculated within the VAMP module of Materials Studio with the COSMO solvation method.

The cavity surface or solvent accessible surface of the dyes was obtained using the DMOL<sup>3</sup> module within the Materials Studio software.<sup>33</sup> DMOL<sup>3</sup> includes COSMO-solvation controls, which allow for the treatment of solvation effects. Cavity surface or solvent accessible surface is the surface area of molecules that is accessible to the solvent. The cavity surface is obtained as a superimposition of spheres centered at the atoms, discarding all parts lying on the interior part of the surface. The spheres are represented by a discrete set of points, the so-called basic points. Eliminating the parts of the spheres that lie within the interior part of the molecule thus amounts to eliminating the basic grid points that lie in the interior of the molecule. The radii of the spheres are determined to be the sum of the van der Waals radii of the atoms of the molecule and the probe radius. The surviving basic grid points are then scaled to lie on the surface generated by the spheres of van der Waals radii alone. The basic points are then

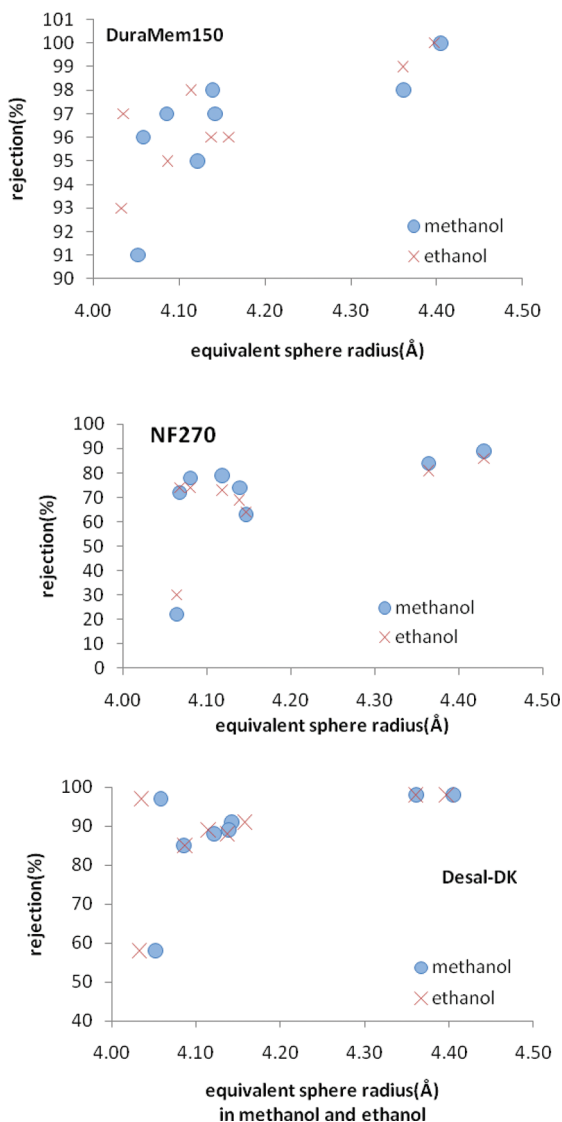


**Figure 5.** Retention curves as a function of equivalent sphere radius for the membranes DuraMem150, NF270, and Desal-DK. (applied pressure: 20 bar). Retentions of dyes are presented for both methanol and ethanol. Figure 6 indicates that there is not an overall good correlation between retention value and equivalent surface radius. From left to right (methanol): Disperse Black 9, Disperse Orange 1, Disperse Red 1, Disperse Red 19, Disperse Red 13, Disperse Orange 25, Disperse Red 1 methacrylate, Disperse Red 13 methacrylate. From left to right (ethanol): Disperse Black 9, Disperse Orange 1, Disperse Red 1, Disperse Red 13, Disperse Red 19, Disperse Orange 25, Disperse Red 1 methacrylate, Disperse Red 13 methacrylate.

collected into segments, which are also represented as discrete points on the surface. The screening charges are located at the segment points.<sup>43</sup>

Amorphous cell models of all azo dyes except the methacrylate dyes were constructed, using periodic boundary conditions, through the procedure mentioned earlier. The initial constructed amorphous cells were subjected to a series of energy minimization to reach a minimal potential energy condition and to achieve ideal molecule packing in the amorphous cell. Forcite cohesive energy density task is used to calculate the solubility parameter in the Materials Studio software.<sup>33</sup>

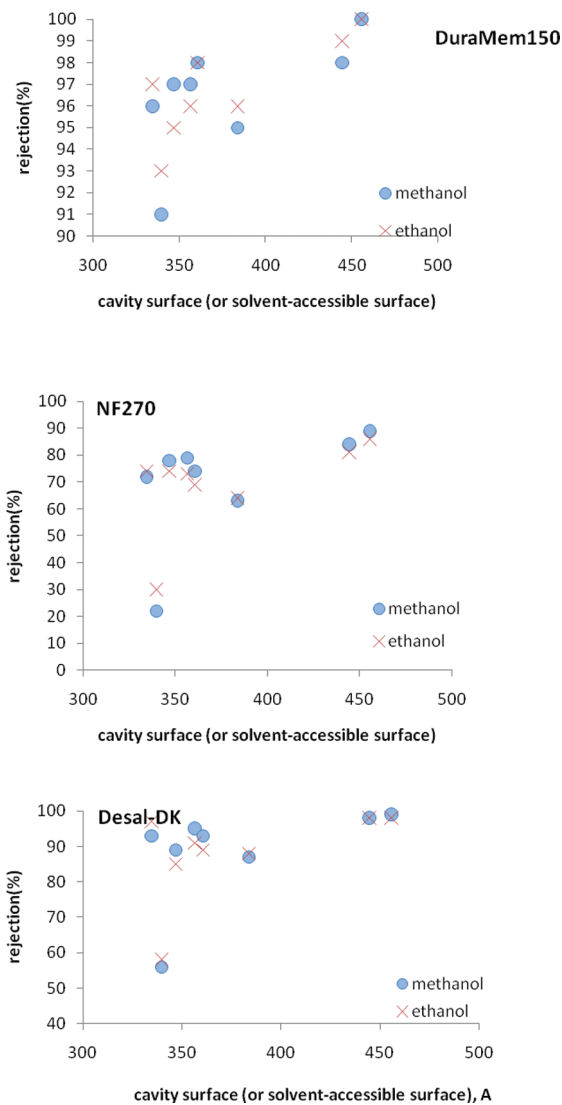


**Figure 6.** Retention curves as a function of cavity surface (or solvent-accessible surface) for the membranes DuraMem150, NF270, and Desal-DK. (applied pressure: 20 bar). Retentions of dyes are presented for both methanol and ethanol. From left to right: Disperse Orange 1, Disperse Black 9, Disperse Red 1 methacrylate, Disperse red 1, Disperse Red 13 methacrylate, Disperse Orange 25, Disperse Orange 13, Disperse 19.

### 3. RESULTS AND DISCUSSION

**Flux, Flux Decline, Normalized Flux, and Retention.** Table 4 summarizes the experimental relative flux, normalized flux, and retention of the different membranes used in this research. The mean values of three independent experiments are presented. Experimental measurements were repeated with a new membrane sheet if the variation was over 5%. The Duramem 150 membrane has the highest retention, which is logical as this membrane has the smallest MWCO. The retentions of the other membranes, which had a similar MWCO, were similar.

**Influence of Molecular Weight and Molecular Size on Retention.** Figure 4 shows the retention of all dyes as a function of molar mass for the three membranes at a transmembrane pressure of 20 bar. Retention values of dyes are shown in Figure 4 for both methanol and ethanol.

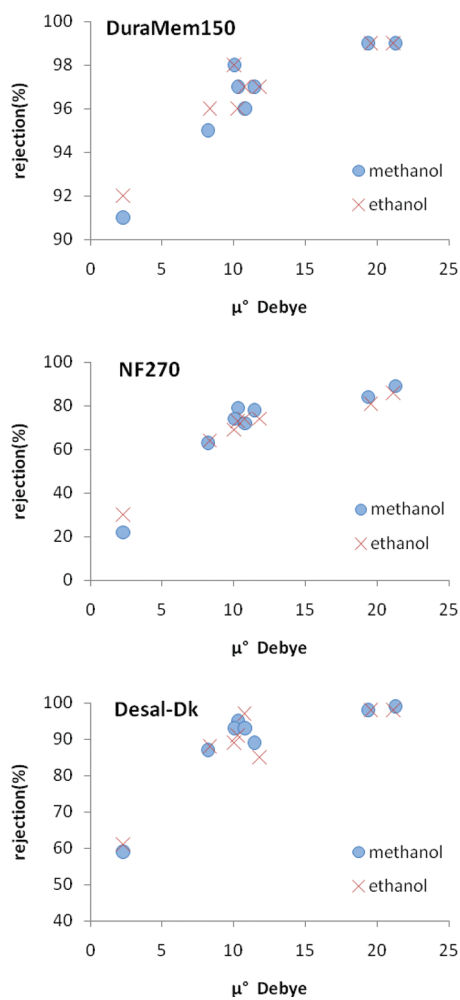


**Figure 7.** Retention curves as a function of dipole moments (Debye) for the membranes DuraMem150, NF270, and Desal-Dk. (applied pressure: 20 bar). Retentions of dyes are presented for both methanol and ethanol. From left to right: Disperse Black 9, Disperse Red 19, Disperse Red 13, Disperse Orange 25, Disperse Orange 1, Disperse Red 1, Disperse Red 1 methacrylate, Disperse Red 13 methacrylate.

From figure 4 it appears that the retention curves are somewhat scattered for dyes with molar mass between 300 and 350 Da. From Figure 4 it is obvious that retention values increase sharply for Duramem150 and Desal-Dk, and retention of Disperse Red 13 methacrylate in methanol and ethanol is >99%. For NF270, the retention curves increased gradually and reach 89% retention for Disperse red 13 methacrylate in methanol and 86% in ethanol. Only the retention of Disperse Black 9 appears to be an anomaly. A hypothesis for this will be presented later (see Dipole Moment of Dyes and Total Electron Density).

Table 5 presents the calculated dimensions in terms of van der Waals surface and occupied volume for all azo dyes in methanol and ethanol. In methanol and ethanol, azo dyes form some hydrogen bonds with  $-\text{OH}$  groups. Therefore, the actual size of the dyes changes in these solvents.

Figure 5 presents the retention value versus the equivalent sphere radius in methanol and ethanol. A comparison between Figures 4 and 5 indicates that the equivalent sphere radius is not a better parameter than the molecular weight to describe retentions. It is illustrated in Figure 5 that all equivalent sphere radii

vary between 4.0 to 4.2 Å, except for the methacrylate dyes. The correlation of retentions is only slightly changed by using size parameters other than molar mass. It has been shown (Figure 5) that a good correlation exists between the studied size parameters and retention while the differences are large enough (equivalent sphere radius difference  $> 0.5$  Å). The equivalent sphere radii for Disperse Red 1, Disperse Orange 1, and Disperse Black 9 are very similar, between 4.05 and 4.10 Å in vacuo and in solvent. However, the retention of Disperse Red 1 and Disperse Orange 1 is much higher than that of Disperse Black 9, which indicates that, apart from size, another parameter also influences the retention. Figure 6 presents the retention of dyes versus the cavity surface. Cavity surface or solvent accessible surface cavity surface is the surface area of molecules that is accessible to the solvent.

The cavity surfaces of Disperse Red 1, Disperse Orange 1, and Disperse Black 9 are similar, which indicates that cavity surface is also not the only parameter influencing the retention. Generally, the correlation of retention with molar mass is slightly different than that with size parameters with a physical meaning such as Stokes diameter, equivalent molar diameter, or cavity surface (solvent-accessible surface). Therefore, molar mass remains useful for the description of retention. Van der Bruggen et al.<sup>4</sup> also came to the same conclusion for nanofiltration of different solutes in water. The authors claimed that molar mass is a practical parameter for the description of retention. However, a physical parameter is necessary for modeling the solute retention, since solute transport cannot be described with molar mass. It has been shown that a good correlation exists between the studied size parameters and retention;<sup>4</sup> therefore, they can be used in a model. Disperse Black 9 has the lowest molar mass and other size parameters of all dyes used. However, the difference between any size descriptor for this dye with the same descriptor for the other dyes does not explain such differences in retentions. For example, the molar mass and other size parameters of Disperse Orange 1 or Disperse Red 1 are very similar to those of Disperse Black 1, but the retentions are much higher than for Disperse Black 1, which clearly indicates the effect of another parameter on the retention of dyes in methanol and ethanol.

**Dipole Moment of Dyes and Total Electron Density.** Figure 7 presents the retention versus the dipole moment of the dyes. It appears that the highest dipole moments consistently show a higher retention than molecules of approximately the same dipole moments. For all membranes, the retention of Disperse Black 9 is significantly lower than that for Disperse Orange 1 or Disperse Red 1.

The effect of the dipole moment was already found by Van der Bruggen et al.<sup>4</sup> It was suggested that the polarity of the molecule had an influence on the orientation of the molecule relative to the membrane. In the case of elongated molecules, a more perpendicular orientation relative to the membrane can dramatically decrease the apparent size and thus the retention of a molecule. Santos et al.<sup>44</sup> used the preferential orientation as a fitting parameter in their model. They found that the preferential orientation of elongated compounds became more perpendicular, and consequently the retentions dropped if these molecules had only one polar end group compared to molecules with a polar group at each end of the molecule. They did not calculate the dipole moment, but it is clear that their results would support an orientation more perpendicular to the

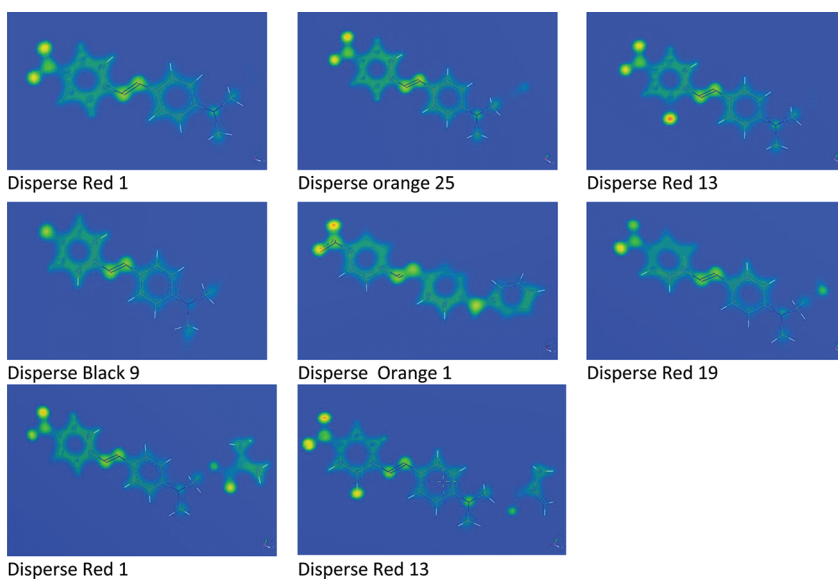


**Figure 8.** The electron density field of the azo dyes optimized with the VAMP module.

membrane and thus a lower retention for molecules with a lower dipole moment.

The origin of this preferential orientation has to be sought in the force balance and more specifically the torque balance on the compounds. The main forces involved are the friction force with the membrane as well as the friction force with the solvent or, equivalently, the drag force of the solvent molecules on the compound. The strongest intermolecular forces after charge interactions are hydrogen bonds, and these will probably dominate the torque balance on a molecule. Due to hydrogen bonding, a polar solvent will interact much more with the polar end groups of an elongated molecule than with a nonpolar backbone. The nonpolar backbone will tend to interact more with the membrane, as the membrane is generally less polar than the solvent. In the case of only one polar end group and a nonpolar backbone, the center of all drag forces of the solvent molecules on the compound will be near this end group while the center of friction forces with the membrane will be near to the center of mass of the backbone. An upward membrane friction force near the center of mass and a downward solvent drag force near the polar head will stabilize an orientation more or less parallel to the average solvent velocity, or equivalently perpendicular to the membrane. This orientation will decrease the apparent size or the friction with the membrane, resulting in a lower retention. If two polar end groups are present at opposite ends of a nonpolar backbone, the distance between the center of membrane friction forces and the center of drag forces will become very small, creating an unstable situation with no preferential orientation, similarly to a floating body with a center of mass very near the center of buoyant forces. In this case, the apparent size or friction with the membrane will be larger, translating into a larger retention.

Hydrogen bonds are formed by strongly electronegative atoms. The presence of these atoms can be derived indirectly by the electron density (Figure 8). The electron density field of the azo dyes optimized with VAMP is shown in Figure 8. A hydrophilic molecule or portion of a molecule is one that is typically charge-polarized or has high electron density and is

capable of hydrogen bonding, enabling it to dissolve more readily in a polar solvent (water, methanol, ethanol) than in oil or other nonpolar solvents. Brighter parts in Figure 8 indicate a higher electron density, which represents the hydrophilic part of each molecule.

Due to hydrogen bonding, the interaction of methanol and ethanol with hydrophilic groups of a molecule will be larger than with other groups. The center of the drag forces will therefore not be near the center of mass but near the more hydrophilic part of the molecule. The reduced interaction with methanol/ethanol for hydrophobic parts of the molecule increases the possible interaction with the membrane. The center of friction force will therefore be near the more hydrophobic part of the molecule. Solvent-coupled transport in combination with membrane friction could thus also generate torque forces and influence the orientation and retention of an elongated molecule. Independent of the type and amplitude of forces acting on the molecule, it is obvious that the torque on the molecule will decrease with increasing molecular symmetry. An elongated molecule with one hydrophilic end group will have a more perpendicular orientation than the same molecule with two identical hydrophilic end groups at the opposite side of the chain. The molecule with one hydrophilic end group will therefore have a lower retention. Only Disperse Black 9 has an  $-NH_2$  end group, in contrast to the other dyes with  $-NO_2$ , leading to a lower hydrophilicity of these dyes compared to the other (one light green spot compared to three light green spots). The lower retention of Disperse Black 9 compared to the other dyes supports the proposed hypothesis.

**Effect of the Solubility Parameter.** The (Hildebrand) solubility parameter is a molecular descriptor that characterizes the solubility based on the cohesive energy. Materials with similar solubility parameters will dissolve in each other or at least have a high affinity toward each other.

## THEORETICAL SOLUBILITY PARAMETERS

The solubility parameters of azo dyes were calculated using a group contribution method. In this way the contribution of each

**Table 6. Group Contributions to the Cohesive Energy and Molar Volume Used to Estimate the Solubility Parameter for Common Dyes<sup>43</sup>**

group	$E_{coh}$ (J/mol)	$V_m$ (cm <sup>3</sup> /mol)
-CH <sub>3</sub>	4707	33.5
-CH <sub>2</sub> -	4937	16.1
-CH	3431	-1
C	1464	-19.2
-H <sub>2</sub> C=	4310	28.5
-CH=	4310	13.5
C=	4310	-5.5
HC≡	3849	27.4
-C≡	7071	6.5
phenyl	31924	71.4
phenylene (o, m, p)	31924	52.4
phenyl (trisubstituted)	31924	33.4
phenyl (tetrasubstituted)	31924	14.4
phenyl (pentasubstituted)	31924	-4.6
phenyl (hexasubstituted)	31924	-23.6
ring closure 5 or more atoms	1046	16
ring closure 3 or 4 atoms	3138	18
conjugation in ring for each double bond	1674	-2.2
-COOH	27614	28.5
-CO <sub>2</sub> -	17991	18
-CO-	17364	10.8
-CONH-	33472	9.5
-NH <sub>2</sub>	12552	19.2
-NH-	8368	4.5
N	4184	-9
-N=	11715	5
-N=N-	4188	0
-CN	25522	24
NO <sub>2</sub> (aromatic)	15355	32
-O-	3347	3.8
-OH	29790	10
-OH (disubstituted or on adjacent C atoms)	21840	13
S	14142	12
-SO-	39140	0
-SO <sub>4</sub> -	28451	31.6
-F	4184	18
-Cl	11548	24
-Br	15481	30
-I	19037	31.5

functional group and each fragment of the parent chemical structure was calculated as part of the overall solubility parameter.

$$\delta = \left( \frac{\sum E_{coh_i}}{\sum V_{mi}} \right)^{1/2}$$

$\delta$  is the solubility parameter of a molecule,  $E_{coh_i}$  is the cohesive energy for the  $i$  functional group on the molecule, and  $V_{mi}$  is its molar volume. Table 6 lists the cohesive energy and molar volume values used to estimate the solubility parameter for common dyes.

**Table 7. Solubility Parameters from MD Simulations and Group Contribution Methods (MPa<sup>0.5</sup>)**

	solubility parameter group contribution method	solubility parameter MD simulation
Disperse Red 1	24.96	21.66
Disperse Orange 25	23.82	25.94
Disperse Red 13	25.70	27.62
Disperse Black 9	27.84	23.10
Disperse Orange 1	24.11	27.11
Disperse Red 19	28.04	30.00

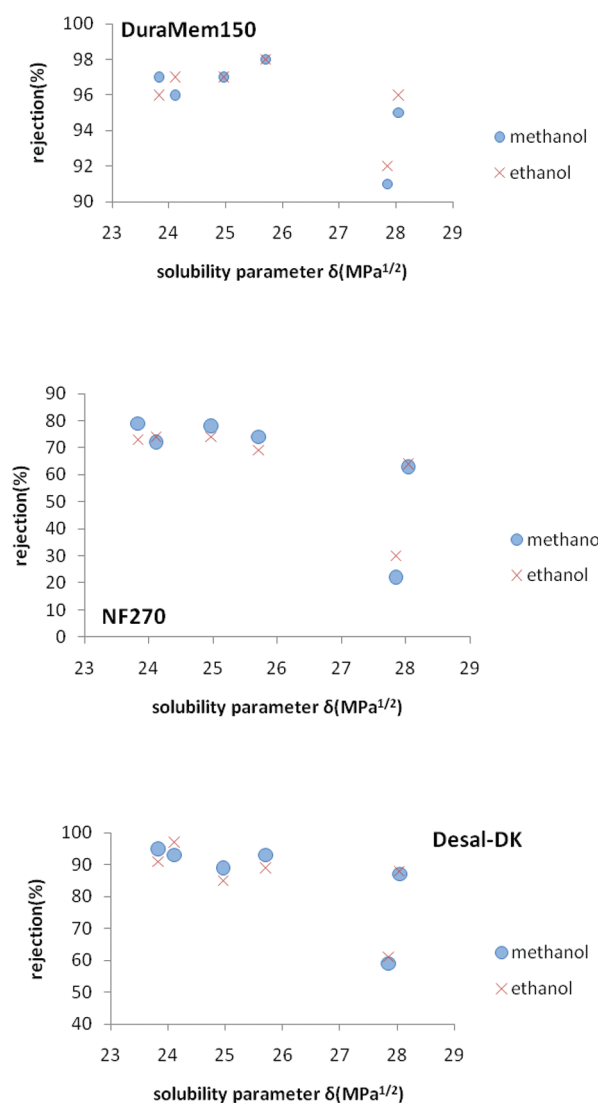


**Figure 9.** Retention values as a function of solubility parameter calculated by the group contribution method for the membranes DuraMem150, NF270, and Desal-DK. (applied pressure: 20 bar). Retentions of dyes are presented for both methanol and ethanol. From left to right: Disperse Orange 25, Disperse Orange 1, Disperse Red 1, Disperse Red 13, Disperse Black 9, Disperse Red 19.

Table 7 compares the solubility parameter values for all azo dyes, except methacrylate dyes, computed from the MD

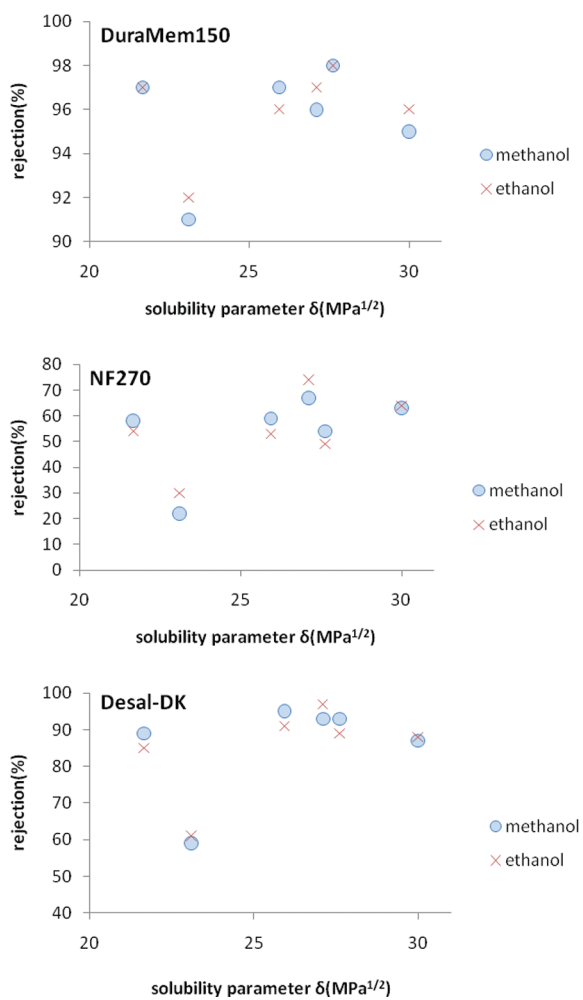


**Figure 10.** Retention curves as a function of solubility parameter calculated by MD for the membranes DuraMem150, NF270, and Desal-DK. (applied pressure: 20 bar). Retentions of dyes are presented for both methanol and ethanol. From left to right: Disperse Red 1, Disperse Black 9, Disperse Orange 25, Disperse Orange 1, Disperse Red 13, Disperse 19.

simulations at 298 K with the values calculated by using the group contribution method. As seen in Table 7, the solubility parameter values computed from MD simulations is logically similar to the one calculated using the group contribution methods. From Table 7 it was concluded that the two methods yielded comparable values.

The effect of the solubility parameter on the retention of dyes is shown in Figure 9. In an amorphous polymeric structure such as the membranes used in this study, solute and solvent molecules would interact and dissolve in the polymer matrix and pass through it.<sup>45</sup> Generally, the closer the solvent/solute and membrane solubility parameters are to one another, the stronger the solvent/solute–polymer interactions that take place. A higher difference for the solubility parameter would indicate that the interaction between solvent/solute and polymer is small. Membrane solubility parameters can be calculated from group contribution methods if the specific structure of the membrane repeat unit is identified. Unfortunately, for commercial membranes this value can only be estimated. Silva et al.<sup>46</sup> calculated the solubility values for typical

PIs used for forming OSN membranes such as Lenzing P84 (26.8 MPa<sup>1/2</sup>) and Matrimid 5218 (23.2 MPa<sup>1/2</sup>) using a group contribution method.<sup>38</sup> The solubility parameter of aromatic PA is also reported in the literature as 25 MPa<sup>1/2</sup>.<sup>47</sup> The solubility parameter does not vary significantly between these membranes. The same conclusion can be drawn for azo dyes, which have relatively similar solubility parameters. Excluding Disperse Black 9 from Figure 9, no relation between the solubility parameter calculated by the group contribution method and retention was observed. Both membrane and dyes have similar properties, which demonstrate their affinity toward each other. However, higher retentions in all cases except Disperse Black 9 could be due to the higher dipole moment of the other dyes (part 3), while the solubility parameter is not the real parameter influencing the retention here.

Figure 10 presents the retentions as a function of solubility parameters of the dyes, calculated by MD simulations. The correlation of retention value is not better by using the solubility parameter calculated by MD. Disperse Black 9 has the solubility parameter value that is the closest to the value of the membranes. This similarity may be the reason for the lower retention of this dye. However, due to the uncertainty about the solubility parameter of the membranes, final conclusions about the effect of the solubility parameter cannot be made.

## CONCLUSION

The current study has demonstrated that a good correlation exists only between retention and the dipole moment of the azo dyes solutes with molecular weight around 350 Da. Molar mass, equivalent molar diameter, and calculated cavity surface seem to have a good correlation, while the sizes of solutes are similar to each other. When the difference between molecular molar mass or different size parameter of solutes increases, these parameters present better correlations. A slightly better presentation of size parameter compared to the MWCO has been observed.

Applying MD simulation, an effect of polarity through the dye dipole moment in methanol and ethanol on retention was found. Disperse Black 9 with a lower dipole moment has lower retention compared to more hydrophilic dyes. This effect, which is independent of the membrane characteristics, can be explained by electrostatic interaction directing the dipole toward the membrane or slowing down the dye inside the pores of the membrane.

Furthermore, the retention behavior of azo dyes is also studied by solubility parameter effects. No clear relation between solubility parameter and its effect on retention of dyes has been observed. Generally, for the membrane studied here, a higher or lower retention can be achieved for the solutes with similar molar mass or similar size. The hydrophilicity of the dyes affects the overall position toward the membrane and for the solutes with size close to the membrane pore size, the influence of molecular hydrophobicity was found to be important as well. The differences in retention between ethanol and methanol were generally very small, thus no clear conclusions could be derived about the effect of the solvent.

## ACKNOWLEDGMENT

The Research Council of K. U. Leuven is gratefully acknowledged for financial support of this work (OT/2006/37). The FWO (FONDS Wetenschappelijk Onderzoek) is also gratefully acknowledged for the grant given to Siavash Darvishmanesh for

performing the simulation work at ITM-CNR, ITALY. Parts of the work leading to these results have received funding from the EC's Seventh Framework Programme (FP7/2007-2013) under Grant Agreement No. NMP3-SL-2009-228631, project DoubleNanoMem "Nanocomposite and Nanostructured Polymeric Membranes for Gas and Vapour Separations".

## ■ REFERENCES

- (1) Darvishmanesh, S.; Degreve, J.; Van der Bruggen, B. *Phys. Chem. Chem. Phys.* **2010**, *12*, 13333–13342.
- (2) Schäfer, A.; Fane, A.; Waite, T. *Nanofiltration: Principles and Applications*; Elsevier Advanced Technology: Kidlington, U.K., 2005.
- (3) Van der Bruggen, B.; Määttäri, M.; Nyström, M. *Sep. Purif. Technol.* **2008**, *63*, 251–263.
- (4) Van der Bruggen, B.; Schaep, J.; Wilms, D.; Vandecasteele, C. *J. Membr. Sci.* **1999**, *156*, 29–41.
- (5) de Moura, J. M. L. N.; Gonçalves, L. A. G.; Petrus, J. C. C.; Viotto, L. A. *J. Food Eng.* **2005**, *70*, 473–478.
- (6) Manjula, S.; Subramanian, R. *Crit. Rev. Food Sci. Nutr.* **2006**, *46*, 569–592.
- (7) Hope, E. G.; Abbott, A. P.; Davies, D. L.; Solan, G. A.; Stuart, A. M. *Green Organometallic Chemistry*. In *Comprehensive Organometallic Chemistry III*; Robert, H. C., Mingos, D. M. P., Eds.; Elsevier: Oxford, 2007; pp 837–864.
- (8) Nair, D.; Luthra, S.; Scarpello, J.; White, L.; Freitas dos Santos, L.; Livingston, A. *Desalination* **2002**, *147*, 301–306.
- (9) Scarpello, J. T.; Nair, D.; Freitas dos Santos, L. M.; White, L. S.; Livingston, A. G. *J. Membr. Sci.* **2002**, *203*, 71–85.
- (10) Darvishmanesh, S.; Degrèe, J.; Van der Bruggen, B. *Ind. Eng. Chem. Res.* **2010**, *49*, 9330–9338.
- (11) Darvishmanesh, S.; Degrèe, J.; Van der Bruggen, B. *ChemPhysChem* **2010**, *11*, 404–411.
- (12) Geens, J. Mechanisms and modelling of nanofiltration in organic media. Doctoral Thesis, Katholieke Universiteit Leuven, 2006.
- (13) Geens, J.; Hillen, A.; Bettens, B.; Van der Bruggen, B.; Vandecasteele, C. *J. Chem. Technol. Biotechnol.* **2005**, *80*, 1371–1377.
- (14) Van der Bruggen, B.; Jansen, J. C.; Figoli, A.; Geens, J.; Boussu, K.; Drioli, E. *J. Phys. Chem. B* **2006**, *110*, 13799–13803.
- (15) Van der Bruggen, B.; Jansen, J. C.; Figoli, A.; Geens, J.; Van Baelen, D.; Drioli, E.; Vandecasteele, C. *J. Phys. Chem. B* **2004**, *108*, 13273–13279.
- (16) Machado, D. R.; Hasson, D.; Semiat, R. *J. Membr. Sci.* **1999**, *163*, 93–102.
- (17) Bhanushali, D.; Kloos, S.; Kurth, C.; Bhattacharyya, D. *J. Membr. Sci.* **2001**, *189*, 1–21.
- (18) Reddy, K. K.; Kawakatsu, T.; Snape, J. B.; Nakajima, M. *Sep. Sci. Technol.* **1996**, *31*, 1161–1178.
- (19) Machado, D. R.; Hasson, D.; Semiat, R. *J. Membr. Sci.* **2000**, *166*, 63–69.
- (20) Vankelecom, I. F. J.; De Smet, K.; Gevers, L. E. M.; Livingston, A.; Nair, D.; Aerts, S.; Kuypers, S.; Jacobs, P. A. *J. Membr. Sci.* **2004**, *231*, 99–108.
- (21) Robinson, J. P.; Tarleton, E. S.; Millington, C. R.; Nijmeijer, A. *J. Membr. Sci.* **2004**, *230*, 29–37.
- (22) Whu, J. A.; Baltzis, B. C.; Sirkar, K. K. *J. Membr. Sci.* **1999**, *163*, 319–331.
- (23) Whu, J. A.; Baltzis, B. C.; Sirkar, K. K. *J. Membr. Sci.* **2000**, *170*, 159–172.
- (24) Darvishmanesh, S.; Buekenhoudt, A.; Degrèe, J.; Van der Bruggen, B. *J. Membr. Sci.* **2009**, *334*, 43–49.
- (25) Darvishmanesh, S.; Buekenhoudt, A.; Degrèe, J.; Van der Bruggen, B. *Sep. Purif. Technol.* **2009**, *70*, 46–52.
- (26) Darvishmanesh, S.; Degrèe, J.; Van der Bruggen, B. *Chem. Eng. Sci.* **2009**, *64*, 3914–3927.
- (27) Yang, X. J.; Livingston, A. G.; Freitas dos Santos, L. *J. Membr. Sci.* **2001**, *190*, 45–55.
- (28) Choi, P.; Kavassalis, T. A.; Rudin, A. *Ind. Eng. Chem. Res.* **1994**, *33*, 3154–3159.
- (29) Kavassalis, T. A.; Choi, P.; Rudin, A. *Mol. Simul.* **1993**, *11*, 229–241.
- (30) Simperler, A.; Kornherr, A.; Chopra, R.; Bonnet, P. A.; Jones, W.; Motherwell, W. D. S.; Zifferer, G. *J. Phys. Chem. B* **2006**, *110*, 19678–19684.
- (31) Yang, H.; Ze-Sheng, L.; Qian, H.-j.; Yang, Y.-b.; Zhang, X.-b.; Sun, C.-c. *Polymer* **2004**, *45*, 453–457.
- (32) Rigby, D. *Fluid Phase Equilib.* **2004**, *217*, 77–87.
- (33) Milman, V.; Winkler, B.; Probert, M. *J. Phys.: Condens. Matter* **2005**, *17*, 2233.
- (34) Hofmann, D.; Entrialgo-Castano, M.; Lerbret, A.; Heuchel, M.; Yampolskii, Y. *Macromolecules* **2003**, *36*, 8528–8538.
- (35) Chang, K.-S.; Huang, Y.-H.; Lee, K.-R.; Tung, K.-L. *J. Membr. Sci.* **2010**, *354*, 93–100.
- (36) Wang, X.-Y.; Lee, K. M.; Lu, Y.; Stone, M. T.; Sanchez, I. C.; Freeman, B. D. *Polymer* **2004**, *45*, 3907–3912.
- (37) Takaba, H.; Mizukami, K.; Kubo, M.; Fahmi, A.; Miyamoto, A. *AIChE J.* **1998**, *44*, 1335–1343.
- (38) Smallwood, I. *Handbook of Organic Solvent Properties*; Arnold: London, 2000.
- (39) Kathleen Boussu, J. D. B.; Dauwe, C.; Weber, M.; Lynn, K. G.; Depla, D.; Aldea, S.; Vankelecom, I. F. J.; Vandecasteele, C.; Van der Bruggen, B. *ChemPhysChem* **2007**, *8*, 370–379.
- (40) Hunger, K. *Industrial Dyes: Chemistry, Properties, Applications*; Wiley-VCH: Weinheim, Germany, 2003.
- (41) Clark, T.; Rauhut, G.; Breindl, A. *J. Mol. Model.* **1995**, *1*, 22–35.
- (42) Rauhut, G.; Clark, T.; Steinke, T. *J. Am. Chem. Soc.* **1993**, *115*, 9174–9181.
- (43) Klamt, A.; Schüürmann, G. *J. Chem. Soc., Perkin Trans. 2* **1993**, 799–805.
- (44) Santos, J. L. C.; de Beukelaar, P.; Vankelecom, I. F. J.; Velizarov, S.; Crespo, J. G. *Sep. Purif. Technol.* **2006**, *50*, 122–131.
- (45) Barton, A. F. M. *CRC Handbook of Polymer–Liquid Interaction Parameters and Solubility Parameters*; CRC Press: Boca Raton, FL, 1990.
- (46) Silva, P.; Han, S.; Livingston, A. G. *J. Membr. Sci.* **2005**, *262*, 49–59.
- (47) Sourirajan, S.; Matsuura, T. *Reverse Osmosis and Ultrafiltration*; American Chemical Society: Washington, DC, 1985.